https://doi.org/10.31436/iiumej.v26i1.3259

ANALYSIS OF BRAIN TISSUE POROELASTIC PROPERTIES USING MULTISCALE MODELLING

ABBAS SHABUDIN[1], MOHD JAMIL MOHAMED MOKHTARUDIN[1*], NIK ABDULLAH NIK MOHAMED[2], MOHD AKRAMIN MOHD ROMLAY[3]

[1]*Faculty of Manufacturing and Mechatronic Engineering Technology, Universiti Malaysia Pahang Al-Sultan Abdullah, Pekan, Malaysia*

[2]*Faculty of Engineering, Technology and Built Environment, UCSI University Kuala Lumpur, Kuala Lumpur, Malaysia*

[3]*Faculty of Mechanical and Automotive Engineering Technology, Universiti Malaysia Pahang Al-Sultan Abdullah, Pekan, Malaysia*

**Corresponding author: mohdjamil@umpsa.edu.my*

(Received: 15 April 2024; Accepted: 21 October 2024; Published online: 10 January 2025)

ABSTRACT: Mathematical models are developed to understand ischaemic stroke formation further and achieve treatment effectiveness. The existing poroelastic model of the brain assumed the brain as a homogenized structure with uniform capillary distribution. This paper describes using a multiscale modeling technique known as asymptotic expansion homogenization (AEH) to derive a new poroelastic model of brain tissue. The model consists of a homogenized governing macroscale model with the effective parameters determined from the microscale cell equations. The microscale cell equations are solved on a representative volume element (RVE) comprising brain tissue embedded with a capillary. Here, the effect of capillary tortuosity and radius on the effective parameters, which are the hydraulic conductivity of the capillary and interstitial space ($\boldsymbol{K}$ and $\boldsymbol{G}$), homogenous Biot's coefficient of the blood and interstitial space (α_c and α_t), Young's modulus ($\bar{E}$) and Poisson's ratio ($\bar{\nu}$), are investigated. From the results, it is found that the percentage difference of $\boldsymbol{K}$ is 97.98% with increasing tortuosity, which suggests that $\boldsymbol{K}$ is significantly influenced by the shape of the capillary. Whereas the percentage difference of $\boldsymbol{G}$ is only 0.25%, which shows that it is unaffected by the shape of the capillary. Meanwhile, α_c and α_t decreases and increases with increasing tortuosity, respectively. Both $\bar{E}$ and $\bar{\nu}$ are not significantly affected by tortuosity, as the percentage difference for each is just 0.14% and 0.03%, respectively. In terms of capillary radius, it is found that $\boldsymbol{K}$ increases and $\boldsymbol{G}$ decreases with the increase of radius. Meanwhile, α_c increases with increasing radius while α_t instead shows the opposite trend. The percentage differences of 18.26% and 14.55% are observed for $\bar{E}$ and $\bar{\nu}$, respectively, implying that both parameters are significantly affected by the capillary radius. In conclusion, including capillary in the brain model significantly affects the effective parameters. Hence, important properties of the capillary, including shape and size, should be carefully emphasized so that accurate findings can be obtained when solving the poroelastic model of the brain.

ABSTRAK: Model matematik dibangunkan untuk mendapatkan pemahaman lanjut tentang pembentukan strok iskemia supaya keberkesanan rawatan dapat dicapai. Model poroelastik otak yang sedia ada menganggap otak sebagai struktur homogen dengan taburan kapilari yang seragam. Makalah ini menerangkan penggunaan teknik pemodelan multiskala yang dikenali sebagai penghomogenan pengembangan asimtotik (PPA) untuk memperoleh model poroelastik baharu untuk tisu otak. Model ini terdiri daripada satu set model skala makro pentadbir homogen dengan parameter berkesan ditentukan daripada persamaan sel skala mikro. Persamaan sel skala mikro diselesaikan pada satu unsur isipadu perwakilan (RVE)

yang terdiri daripada tisu otak dengan kapilari yang tertanam. Di sini, kesan kelikuan dan jejari kapilari pada parameter berkesan, iaitu kekonduksian hidraulik ruang kapilari dan celahan ($\boldsymbol{K}$ dan $\boldsymbol{G}$), pekali Biot homogen bagi darah dan ruang celahan (α_c dan α_t), modulus Young ($\bar{E}$) dan nisbah Poisson ($\bar{v}$), akan diselidiki. Daripada keputusan yang diperoleh, didapati perbezaan peratusan $\boldsymbol{K}$ ialah 97.98% dengan peningkatan kelikuan, yang menunjukkan bahawa $\boldsymbol{K}$ dipengaruhi oleh bentuk kapilari secara signifikan. Manakala peratusan perbezaan $\boldsymbol{G}$ hanyalah 0.25% menunjukkan bahawa ia tidak dipengaruhi oleh kelikuan. Sementara itu, α_c dan α_t masing-masing menurun dan meningkat dengan peningkatan kelikuan. Kedua-dua $\bar{E}$ dan $\bar{v}$ tidak terjejas dengan ketara oleh kelikuan kerana perbezaan peratusan bagi setiap satu ialah masing-masing hanya 0.14% dan 0.03%. Dari segi jejari kapilari pula, didapati $\boldsymbol{K}$ bertambah dan $\boldsymbol{G}$ berkurangan dengan pertambahan jejari. Sementara itu, α_c meningkat dengan peningkatan jejari, manakala α_t sebaliknya. Peratusan perbezaan 18.26% dan 14.55% diperhatikan untuk $\bar{E}$ dan $\bar{v}$ menunjukan bahawa kedua-dua parameter dipengaruhi dengan ketara oleh jejari kapilari. Kesimpulannya, kemasukan kapilari dalam model otak mempunyai kesan yang ketara terhadap parameter berkesan. Oleh itu, sifat penting kapilari termasuk bentuk dan saiz harus ditekankan dengan teliti supaya penemuan yang tepat boleh diperolehi apabila menyelesaikan model poroelastik otak.

KEYWORDS: *Brain Tissue, Poroelastic Properties, Asymptotic Expansion Homogenization, Multiscale Modelling*

1. INTRODUCTION

The brain is a highly vascularized organ, making any computational modeling approach to include all the microvessels difficult [1]. The main problem is the computational cost, which can drastically increase with the number of microvessels in the model. According to Linninger et al., recent computational work can perform computation for 25,000 microvessels within a 30 mm^3 cube, and this, however, still does not represent a complete human brain [2]. Computer simulation of a brain with capillary networks is also time-consuming, so the model must be simplified.

Poroelastic model is an example of a modeling technique that models the interaction between these different phases in the brain tissue, such as the interstitial fluid, blood, and brain cells, and it has been used to study various brain diseases, such as hydrocephalus [3], head injury [4], and brain edema [5, 6]. The brain cell is modeled as a homogeneous linear elastic material. Meanwhile, the interstitial fluid and blood are modeled using Darcy's law, which usually has homogeneous permeabilities. However, this model assumed a homogeneous distribution of pores. This can be revised by considering the complex capillary network in the brain that has various sizes and shapes distributed unevenly in the brain [7]. This inhomogeneity may affect the poroelastic properties of the brain tissue.

To overcome this limitation, the multiscale modeling technique can include the inhomogeneity. Asymptotic expansion homogenization (AEH) is one of the multiscale modeling techniques that has been applied for homogenizing mechanical models of biological tissues and tumors [8-12]. Generally, the technique separates the governing model into homogenized macroscale equations of the brain. The effective parameters of the governing model can be obtained by solving a set of microscale cell equations on a representative volume element (RVE), in which, in the case of the brain, the RVE consists of solid cells and capillaries. The arrangement and dimension of the content of RVE may then affect the effective parameters of the homogenized macroscale equations.

https://doi.org/10.31436/iiumej.v26i1.3259

This article investigates the effect of capillary tortuosity and radius using the AEH technique. Applying the AEH technique will produce a new set of homogenized macroscale equations with the respective effective parameters to be determined by solving the microscale cell equations [13] on an RVE. The RVE used in this article will have a capillary with various radius and tortuosity levels, so its effect on the effective parameters can be investigated.

2. METHODOLOGY

This section discusses the process for obtaining the homogenized macroscale and respective microscale cell equations using the AEH technique. Then, the RVE used will be described.

2.1. Homogenized Governing Macroscale Equation

Assumed that the volume of brain tissue, $\Omega = \Omega_t \cup \Omega_c$, is made up of the poroelastic brain tissue, Ω_t and blood compartment, Ω_c, respectively. The interface between these phases is represented by Γ. Figure 1 illustrates a portion of the brain that is made up of poroelastic tissue and capillary phases. The brain tissue and blood are originally governed by the poroelastic model and Navier-Stokes equations, respectively.

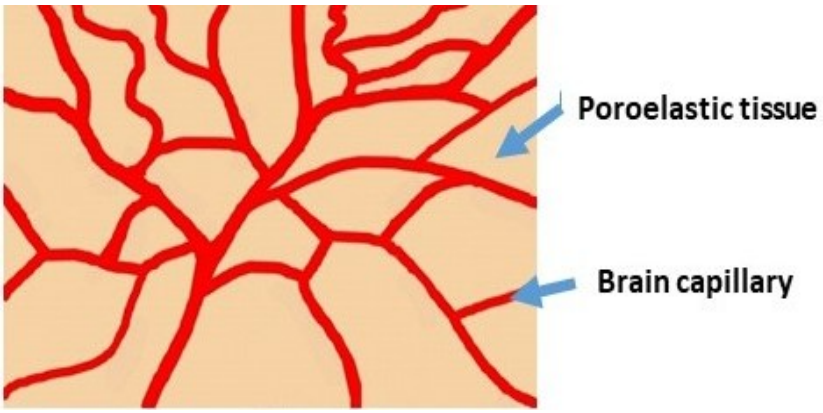

Figure 1. 2D representation of poroelastic brain tissue with capillary.

Assumed that the relationship of the distance between adjacent capillaries d and the normal tissue length, L follows the ratio ϵ as given by Equation (1):

$$\epsilon = \frac{d}{L} \tag{1}$$

which implies that d is much smaller than L. Thus, the length separation between these is very large, allowing for the AEH technique to be applied. Then, two spatial variables y and x for microscale and macroscale, respectively, are defined as:

$$x = \epsilon y \tag{2}$$

Figure 2 illustrates a small portion of the brain consisting of repeating units of brain tissue. Applying the AEH can determine the effective parameters by solving the microscale cell equations on a single RVE without solving the overall brain model. This technique can significantly reduce the computational cost and time.

https://doi.org/10.31436/iiumej.v26i1.3259

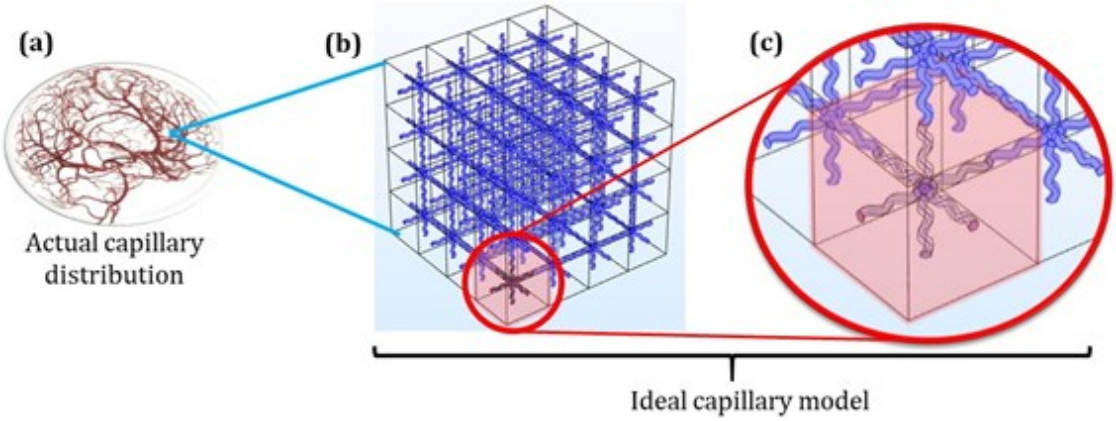

Figure 2. Illustration of repeating units of brain tissue.

2.2. Homogenized Macroscale Equations

The homogenized macroscale stress balance equation is given as:

$$\nabla_{\mathrm{x}} \cdot \sigma_H = 0 \tag{3}$$

Here, the effective stress, σ_H is defined as:

$$\sigma_H = \bar{C} : \nabla_{\mathrm{x}} \boldsymbol{u} - \alpha_c P_c - \alpha_t P_t \tag{4}$$

Here, $\boldsymbol{u}$ is the tissue displacement, P_c is the blood pressure within capillary and P_t is interstitial fluid pressure. Moreover, α_c, and α_t are the Biot's coefficient for blood and interstitial fluid, respectively, and $\bar{C} = \bar{C}(\bar{E}, \bar{\nu})$ is the effective elasticity tensor defined using the effective Young's modulus, $\bar{E}$ and Poisson's ratio, $\bar{\nu}$. These are effective parameters, which can be determined as follows:

$$\bar{C} = \langle (C\boldsymbol{L}C + C) \rangle_{\mathrm{t}} \tag{5}$$

$$\alpha_c = (\phi_c \mathbf{I} - \langle C : \boldsymbol{Q} \rangle_{\mathrm{t}}) \tag{6}$$

$$\alpha_t = (\langle C : \boldsymbol{Q} \rangle_{\mathrm{t}} + \phi_t \mathbf{I}) \tag{7}$$

where ϕ_c and ϕ_t represent the volume ratio for the blood and interstitial fluid, respectively and $\mathbf{I}$ is the identity tensor. Meanwhile, the tensors $\boldsymbol{L}$ and $\boldsymbol{Q}$ can be obtained from the microscale cell equations.

On the other hand, the two fluid pressures are governed by the pressure balance equations as follows:

$$0 = -\nabla_{\mathrm{x}} \cdot \langle \boldsymbol{w}_{\mathrm{c}} \rangle_{\mathrm{c}} 0 + \frac{|\Gamma|}{|\Omega|} \bar{L}_p \Phi_{c \to t} \tag{8}$$

$$0 = -\nabla_{\mathrm{x}} \cdot \langle \boldsymbol{w}_{\mathrm{t}} \rangle_{\mathrm{t}} 0 - \frac{|\Gamma|}{|\Omega|} \bar{L}_p \Phi_{c \to t} \tag{9}$$

where $|\Gamma|$, $|\Omega|$, and $\bar{L}_p$ are the surface area of Γ, the volume of RVE, and the hydraulic conductivity through capillary walls, respectively. Meanwhile, the term $\Phi_{c \to t}$ is defined as follows:

$$\Phi_{c \to t} = P_c - P_t \tag{10}$$

The average fluid velocities $\langle \boldsymbol{w}_c \rangle_c$ and $\langle \boldsymbol{w}_t \rangle_t$ are defined using the respective Darcy's law:

$$\langle \boldsymbol{w}_c \rangle_{\mathrm{c}} = -\boldsymbol{K} \nabla_{\mathrm{x}} P_c \tag{11}$$

https://doi.org/10.31436/iiumej.v26i1.3259

$$\langle \boldsymbol{w}_t \rangle_{\mathrm{t}} = -\bar{k}\boldsymbol{G}\nabla_{\mathrm{x}} P_t \tag{12}$$

Here, the terms $\boldsymbol{K}$ and $\boldsymbol{G}$ the effective parameters can also be obtained from the microscale cell equations. These are the effective hydraulic conductivity for the blood and interstitial fluid. Meanwhile, $\bar{k}$ is the original brain interstitial fluid hydraulic conductivity.

2.3. Microscale Cell Equations

There are four microscale cell equations to be solved on an RVE.

2.3.1 Laplace Cell Equations

The tensor $\boldsymbol{G}$ can be calculated using Eq. (13):

$$\boldsymbol{G} = \phi_t \mathbf{I} - \langle \left(\nabla_{\mathrm{y}} P_t\right)^{\mathrm{T}} \rangle_{\mathrm{t}} \tag{13}$$

where P_t can be determined as follows:

$$\nabla_{\mathrm{y}}^2 P_t = 0 \text{ in } \Omega_{\mathrm{t}} \tag{14}$$

$$\left(\nabla_y \boldsymbol{P}_t\right)\boldsymbol{n} = \boldsymbol{n} \text{ on } \Gamma \tag{15}$$

$$\langle \boldsymbol{P}_t \rangle_t = 0 \text{ in } \Omega_{\mathrm{t}} \tag{16}$$

2.3.2 Stoke's Cell Equations

The tensor $\boldsymbol{K}$ can be calculated using Eq. (17):

$$\boldsymbol{K} = \langle \boldsymbol{W} \rangle_{\mathrm{c}} \tag{17}$$

where $\boldsymbol{W}$ and P_c are obtained as follows:

$$\nabla_{\mathrm{y}}^2 \boldsymbol{W}^{\mathrm{T}} - \nabla_{\mathrm{y}} P_c + \mathbf{I} = 0 \text{ in } \Omega_{\mathrm{c}} \tag{18}$$

$$\nabla_{\mathrm{y}} \cdot \boldsymbol{W}^{\mathrm{T}} = 0 \text{ in } \Omega_{\mathrm{c}} \tag{19}$$

$$\boldsymbol{W}^{\mathrm{T}} = 0 \text{ on } \Gamma \tag{20}$$

$$\langle P_c \rangle_{\mathrm{c}} = 0 \text{ in } \Omega_c \tag{21}$$

2.3.3 One-elastic Cell Equations

The tensor $\boldsymbol{Q}$ can be calculated using Eq. (22):

$$\boldsymbol{Q} = \langle \nabla_{\mathrm{y}} \boldsymbol{a} \rangle \tag{22}$$

where $\boldsymbol{a}$ can be determined as follows:

$$\nabla_{\mathrm{y}} \cdot \left(C \nabla_{\mathrm{y}} \boldsymbol{a}\right) = 0 \text{ in } \Omega_t \tag{23}$$

$$\left(C \nabla_{\mathrm{y}} \boldsymbol{a}\right)\boldsymbol{n} = -\boldsymbol{n} \text{ on } \Gamma \tag{24}$$

$$\langle \boldsymbol{a} \rangle_{\mathrm{t}} = 0 \tag{25}$$

where $\boldsymbol{n}$ is the normal vector to the surface Γ, and $C = C(E, v)$, where E and v are the original brain tissue Young's modulus and Poisson's ratio, respectively.

2.3.4 Six-elastic Cell Equations

The tensor $\boldsymbol{L}$, is defined using Equation (26):

https://doi.org/10.31436/iiumej.v26i1.3259

$$\boldsymbol{L} = \langle \nabla_{\mathbf{y}} A \rangle \tag{26}$$

where A can be calculated as follows:

$$\frac{\partial}{\partial y_j} \cdot \left(\mathbb{C} \frac{\partial A_{kmn}}{\partial y_l} \right) = 0 \text{ in } \Omega_t \tag{27}$$

$$\mathbb{C} \frac{\partial A_{kmn}}{\partial y_l} n_j = -\delta_{im} \delta_{jn} n_j \text{ on } \Gamma \tag{28}$$

$$\langle A \rangle_{\mathrm{t}} = 0 \tag{29}$$

2.4. Capillary RVE

In this study, the RVE used is shown in Figure 3, which is made of a cube and an intersection of cylinders, representing the brain tissue and capillary, respectively. The tortuosity level is determined using the function, $f(s) = Asin(2\pi\omega s/l)$, where ω and A are the capillary tortuosity frequency and amplitude, respectively. Furthermore, Figure 4 shows examples of microstructure with different radius variations. All the analyses performed in this study are dimensionless and solved using the finite element software COMSOL Multiphysics 5.6a.

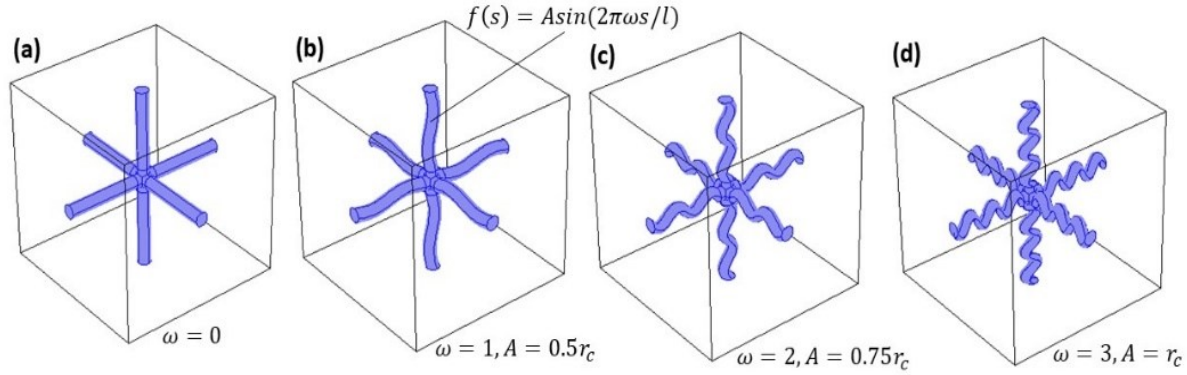

Figure 3. 4 different capillary shapes where (a) consists of straight capillary without tortuosity and (d) represents the most tortuous capillary.

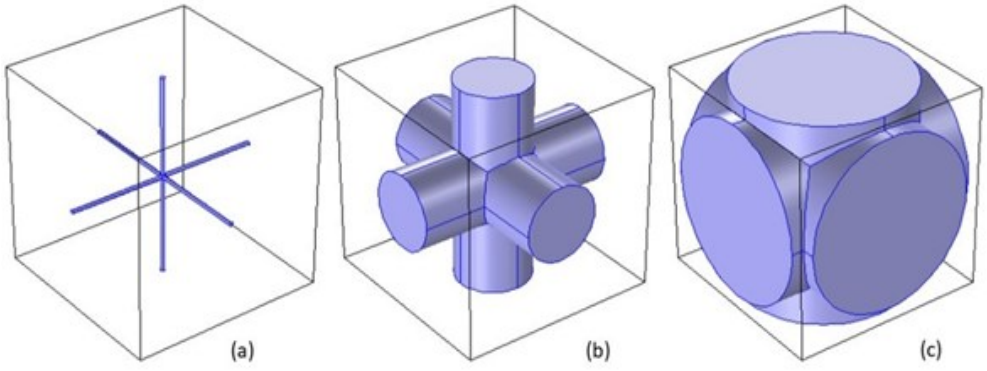

Figure 4. Example of 3 different capillary sizes used for the simulation.

3. RESULTS

The results section will discuss the variations of all the effective parameters with capillary tortuosity in the microstructure RVE.

https://doi.org/10.31436/iiumej.v26i1.3259

3.1. Examples of Microscale Cell Equations Results

Figures 5 and 6 show the example field variables distributions for the four cell equations for microstructure with $\omega = 0$. The results are then used to determine the tensors $\boldsymbol{G}$, $\boldsymbol{K}$, $\boldsymbol{Q}$ and $\boldsymbol{L}$ based on Eqs. (13), (17), (22), and (26).

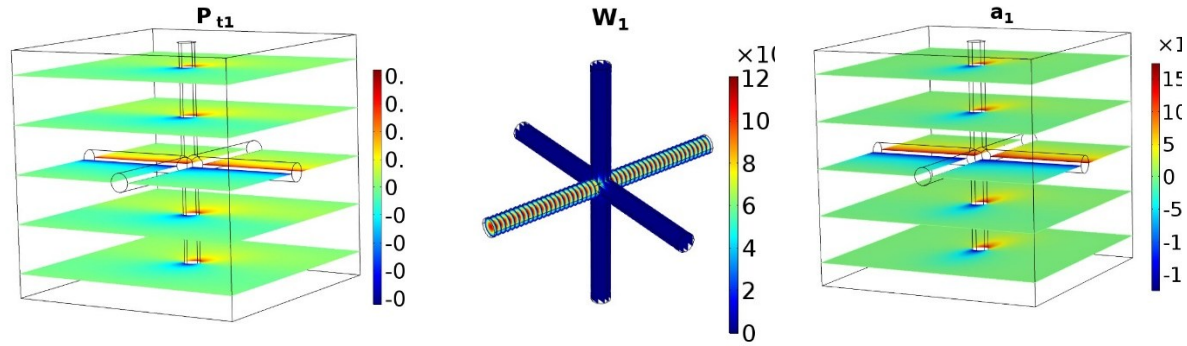

(a) (b) (c)

Figure 5. Example of field variable distribution for (a) Laplace's cell equation, (b) Stokes' cell equation, and (c) One-elastic cell equation.

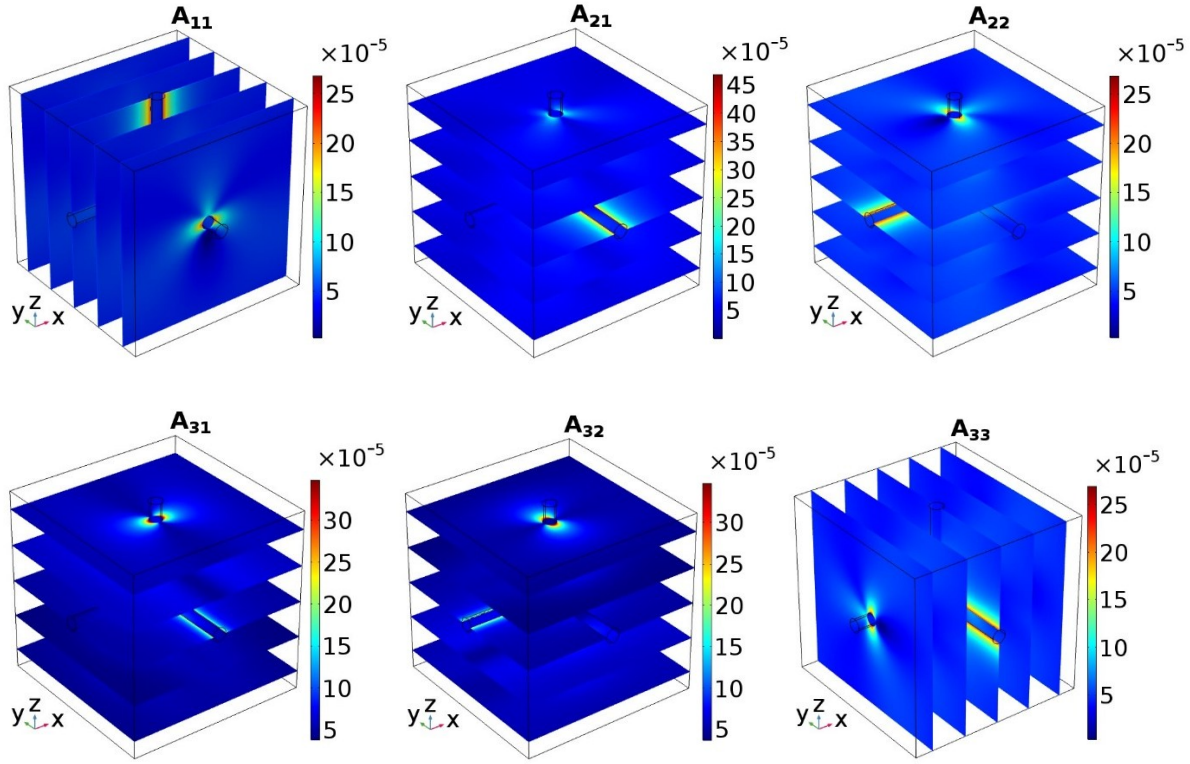

Figure 6. Example of field variable distribution for Six-elastic cell equation.

Figure 7 shows the volume changes in (a) capillary and (b) interstitial space with capillary tortuosity. As the tortuosity increases, the capillary volume decreases. This is because when the capillary is bent at the curve, the space at the curve becomes narrower, as shown in Figure 3(d). Since the volume of a cube is fixed, a smaller volume of capillary results in a larger volume of the interstitial space, as shown in Figure 7(b).

https://doi.org/10.31436/iiumej.v26i1.3259

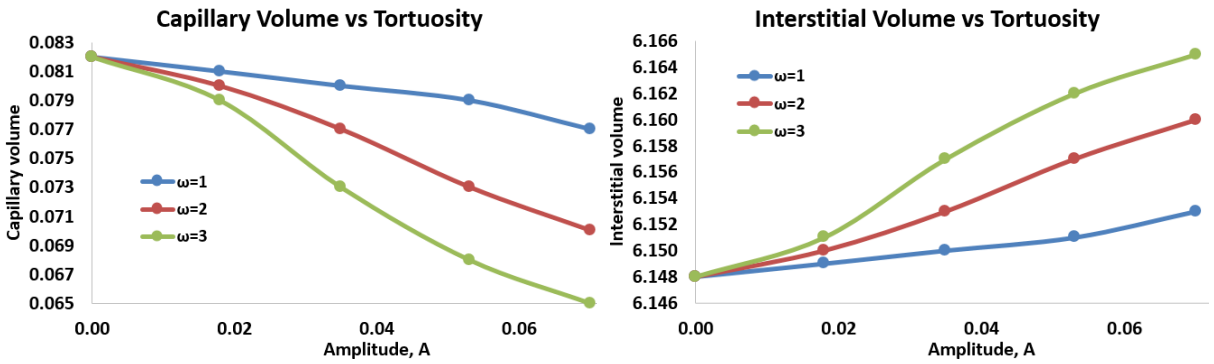

(a) (b)

Figure 7: Capillary and interstitial volume variation for each capillary tortuosity setting.

3.2. Effective Blood Conductivity Tensor, $\boldsymbol{K}$

Figure 8(a) shows that $\boldsymbol{K}$ decreases as the tortuosity increases for $\omega = 1$ to $\omega = 3$. The percentage difference in $\boldsymbol{K}$ between $\omega = 1$ and $\omega = 3$ is 97.98%, and this shows that $\boldsymbol{K}$ is significantly affected by capillary tortuosity. Meanwhile, Figure 8(b) shows that $\boldsymbol{K}$ changes exponentially with increasing microstructure capillary radius. This means that bigger capillaries allow for smoother blood flow due to lower flow resistance [14].

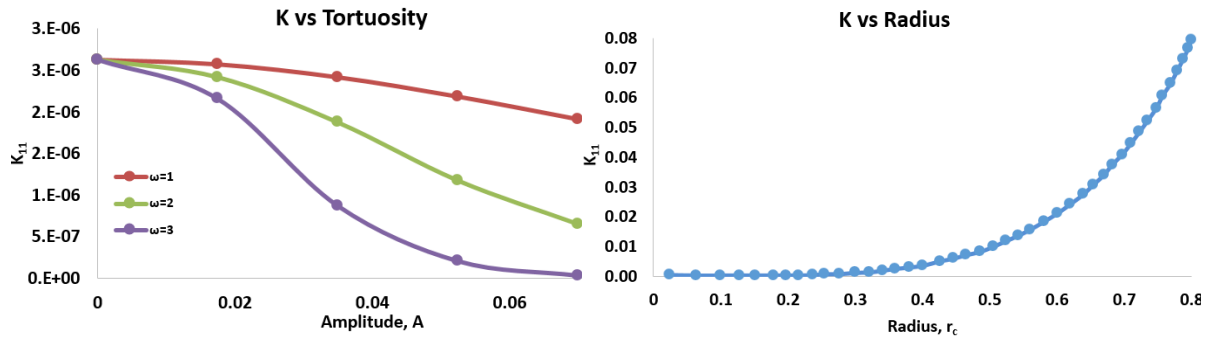

(a) (b)

Figure 8. Graph of $\boldsymbol{K}$ against (a) tortuosity and (b) radius.

3.3. Effective Interstitial Fluid Conductivity Tensor, $\boldsymbol{G}$

Figure 9(a) shows that $\boldsymbol{G}$ increases when tortuosity increases. The percentage difference of $\boldsymbol{G}$ is only about 0.25% between $\omega = 1$ and $\omega = 3$. This shows that $\boldsymbol{G}$ is not affected by capillary tortuosity. Whereas Figure 9(b) shows $\boldsymbol{G}$ decreases with increasing capillary radius. This is because bigger capillary minimizes the interstitial fluid volume and hinders the interstitial fluid flow.

https://doi.org/10.31436/iiumej.v26i1.3259

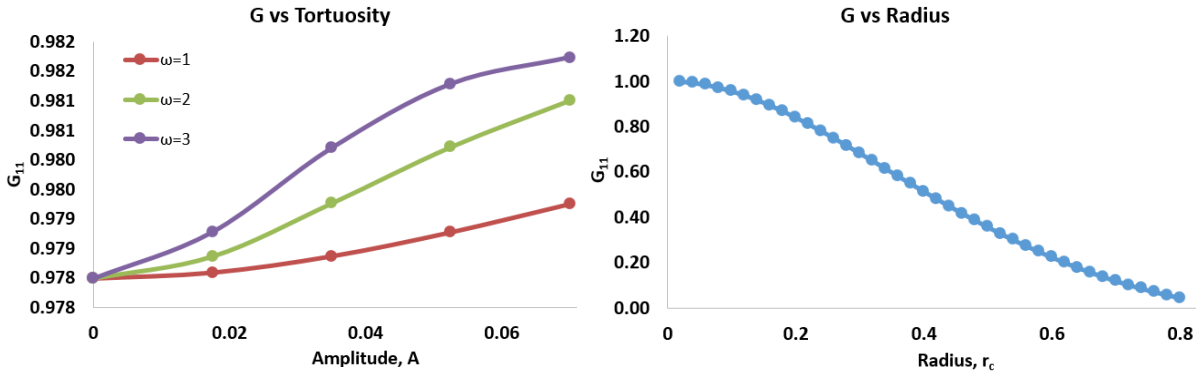

(a) (b)

Figure 9. Effective parameter $\boldsymbol{G}$ against (a) tortuosity and (b) radius.

3.4. Effective Biot's Coefficients, α_c and α_t

In Figure 10(a), the effective blood Biot's coefficient, α_c decreases as the tortuosity increases from ω_1 to ω_3. Modification of capillary tortuosity, which involves changes in capillary volume, will affect α_c because this parameter is dependent on volume changes [11]. Meanwhile, Figure 10(b) shows the effective interstitial fluid Biot's coefficient, α_t, which increases with increasing capillary tortuosity. This implies that more interstitial fluid can be removed from the tissue interstitial by increasing the capillary tortuosity [11].

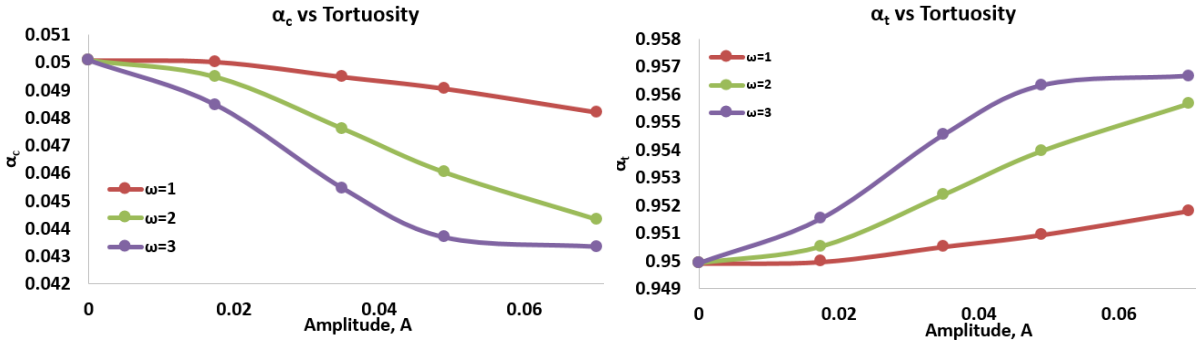

(a) (b)

Figure 10. Graphs of (a) α_c and (b) α_t against tortuosity.

Figure 11 shows the changes of α_c and α_t against radius. As the radius increases, α_c also increases because a bigger capillary volume allows for more blood to be removed from the blood compartment. Meanwhile, α_t decreases as the radius increases. This is because there is a lesser volume of interstitial fluid in the microstructure with a large capillary radius.

https://doi.org/10.31436/iiumej.v26i1.3259

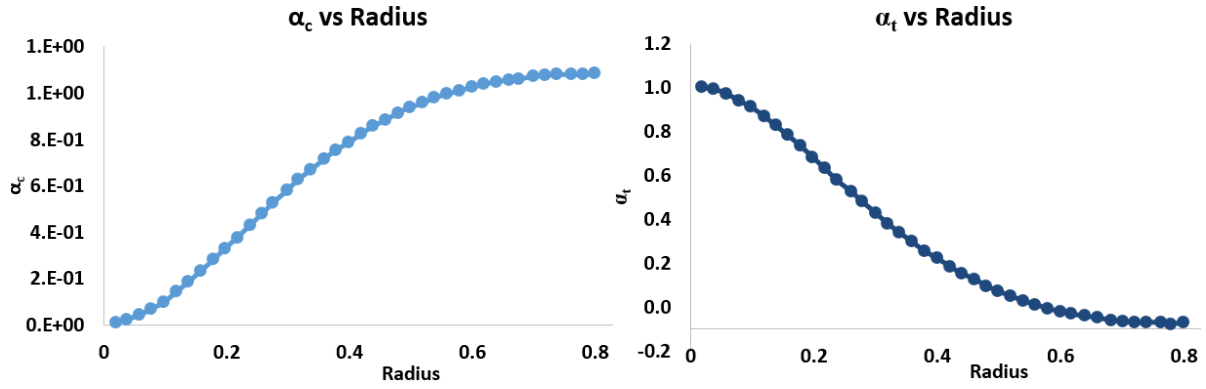

(a) (b)

Figure 11. Graphs of (a) α_c and (b) α_t against radius.

3.5. Effective Moduli

Figure 12 shows the changes in effective moduli with tortuosity. The percentage difference for both $\bar{E}$ and $\bar{\nu}$ are only 0.14% and 0.03%, respectively. The small percentage difference indicates that the tortuosity does not affect the effective elastic moduli. Figure 13 shows the changes in effective moduli with radius. The values of $\bar{E}$ and $\bar{\nu}$ reduce for up to the radius of about 0.4. Then, the values increase as the radius increases up to 0.8. The percentage changes of $\bar{E}$ and $\bar{\nu}$ from the maximum to the minimum values are 18.26% and 14.55%, respectively.

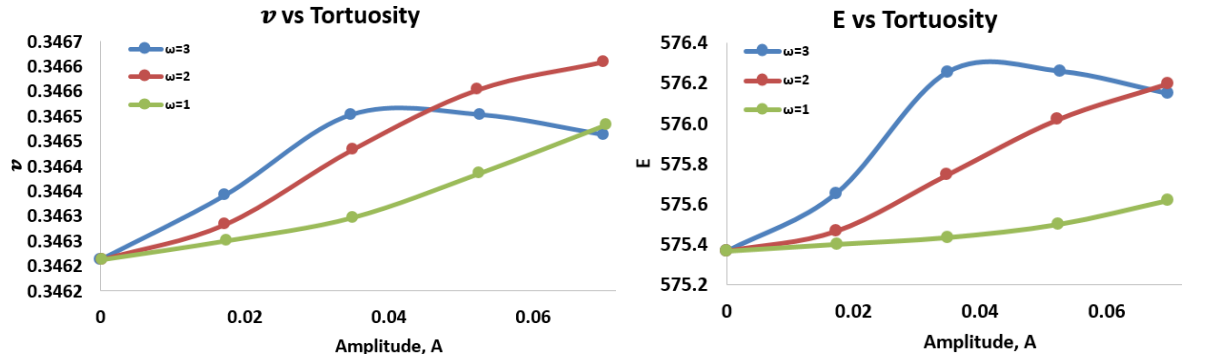

(a) (b)

Figure 12. Graphs of (a) $\bar{\nu}$ and (b) $\bar{E}$ against tortuosity.

As shown in Figure 13, both $\bar{E}$ and $\bar{\nu}$ increase when the capillary tortuosity increases. As mentioned earlier, geometry with high capillary tortuosity has low vascular volume with bigger interstitial tissue volume. Thus, it becomes stiffer (high E) as compared to the geometry with low capillary tortuosity. However, the percentage difference of both $\bar{E}$ and $\bar{\nu}$ from the results are very small, which implies that the tortuosity is insignificantly affecting $\bar{E}$ and $\bar{\nu}$. When varying the radius, it is expected that both $\bar{E}$ and $\bar{\nu}$ decrease as the radius increases since the geometry becomes more porous. However, the simulation outcome only meets our expectations for a radius smaller than 0.4. After 0.4, $\bar{E}$ and $\bar{\nu}$ increase with the capillary radius. For capillary radius bigger than 0.4, both $\bar{E}$ and $\bar{\nu}$ are only influenced by the volume of the capillary. Therefore, as the capillary volume is made larger, $\bar{E}$ and $\bar{\nu}$ obtained are also larger.

https://doi.org/10.31436/iiumej.v26i1.3259

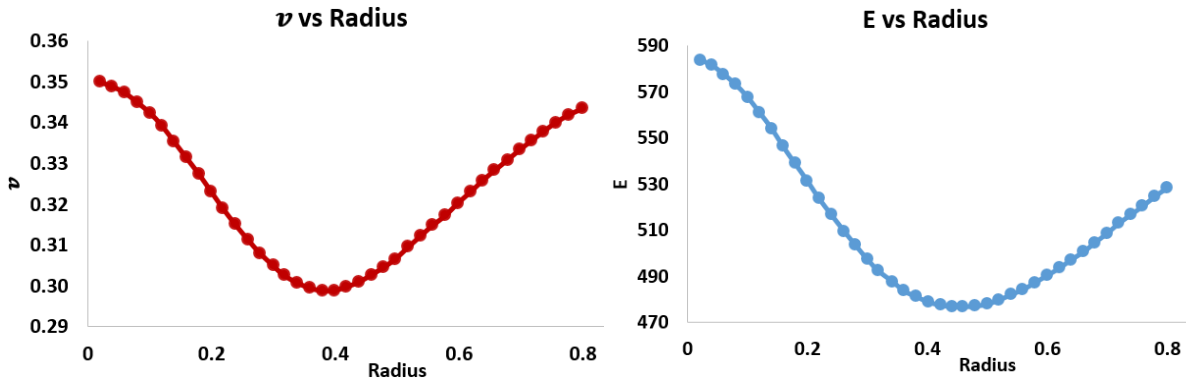

(a) (b)

Figure 13. Graphs of (a) $\bar{v}$ and (b) $\bar{E}$ against radius.

4. DISCUSSION

In this study, the AEH technique was used to derive the microscale cell equations to determine effective parameters for the homogenized macroscale governing equations of the brain. The effective blood hydraulic conductivity, $\boldsymbol{K}$ describes the ability of blood to move through the capillaries [15], in which it depends on several factors, such as the particle size, surface roughness, dimension, structure, and the interconnection between capillaries [16]. The value $\boldsymbol{K}$ obtained here shows a decreasing trend against the capillary tortuosity. The blood flow within a highly tortuous capillary becomes more difficult due to higher flow resistance compared to a less tortuous capillary, resulting in a lower $\boldsymbol{K}$. A similar argument applies to the capillary radius, as can be seen from the results that a bigger capillary has a higher $\boldsymbol{K}$ due to lower flow resistance. Furthermore, the flow resistance is inversely proportional to the radius, following Poiseuille's law [17]. Both tortuous and capillary with small radii have significantly low $\boldsymbol{K}$. These conditions can be used to model blood flow disruption at the macroscale level, representing an ischaemic condition.

Meanwhile, the effective interstitial fluid hydraulic conductivity, $\boldsymbol{G}$ explains the ability of the interstitial fluid to move through interstitial space. This parameter is also highly dependent on the interstitial volume. As the capillary tortuosity increases, the changes in $\boldsymbol{G}$ are very small. This shows that the tortuosity does not affect the interstitial fluid flow. However, $\boldsymbol{G}$ decreases with increasing capillary radius, implying that $\boldsymbol{G}$ is affected by the capillary lumen size. This situation can be explained by the fixed volume of our geometry used in the simulation. As the size of the capillary increases, it occupies more space in the microstructure RVE and reduces the volume of the interstitial fluid. This causes the interstitial fluid flow to become more difficult, hence lowering the hydraulic conductivity [11].

The tensors $\boldsymbol{Q}$ and $\boldsymbol{L}$ have no physical meaning, but it is required in determining the parameters α_c and α_t as well as the effective elastic moduli. Biot's coefficient is a parameter that measures the ratio of the fluid volume squeezed out to the volume change in the poroelastic medium under compression while allowing the fluid to escape [18]. This means that the coefficient depends on the microstructure RVE and capillary volumes. High tortuosity creates a smaller volume of capillary compared to a straight one [8]. This validates our findings whereby α_c decreases and α_t increases with increasing capillary tortuosity. Similarly, for varying radii, a capillary with a bigger radius has greater vascular volume, and hence, α_c and α_t increases and decreases, respectively.

Meanwhile, the effective elastic moduli calculated here are the effective Young's modulus, $\bar{E}$ and Poisson's ratio, $\bar{\nu}$. Young's modulus is defined as the ratio of the applied axial stress to the induced local axial strain in a solid material [19], whereas Poisson's ratio provides a measure of tissue compressibility [20]. Our findings show that the effective elastic moduli changes with the capillary tortuosity and radius. Changes in $\bar{E}$ and $\bar{\nu}$ in biological tissues may be used to indicate the initiation of brain pathological conditions [20]. Hence, sufficient information on these parameters could be used to diagnose a particular brain disease better.

5. CONCLUSION

Application of AEH technique has produced the homogenized macroscale equations with respective microscale cell problems, which are then solved a brain geometry with embedded capillary inside to obtain parameter $\boldsymbol{K}$, $\boldsymbol{G}$, α_c, α_t, $\bar{E}$ and $\bar{\nu}$. The relationship between each parameter and the shapes and sizes of capillaries has been investigated and analyzed. It is found that the value of $\boldsymbol{K}$ is affected by the shape (tortuosity), meanwhile $\boldsymbol{G}$, $\bar{E}$, and $\bar{\nu}$ are affected by the size of the capillary. Only α_c and α_t are influenced by both shape and size. In short, the addition of capillaries greatly impacts the outcome of the simulation of the human brain. Since stroke formation involves the reduction of blood flow in the capillary, all important properties of the capillary should be precisely emphasized so that the simulation outcomes can be improved and used to solve the macroscale equations in a bigger brain geometry.

ACKNOWLEDGEMENT

This research is supported by the UMP Fundamental Research Grant (RDU220367) and the UMP International Publication Grant (RDU203302).

REFERENCES

[1] Peyrounette, M., et al., Multiscale modelling of blood flow in cerebral microcirculation: Details at capillary scale control accuracy at the level of the cortex. PloS one, 2018. 13(1): p. e0189474.

[2] Linninger, A., et al., Cerebral microcirculation and oxygen tension in the human secondary cortex. Annals of biomedical engineering, 2013. 41(11): p. 2264-2284.

[3] Tully, B. and Y. Ventikos, Cerebral water transport using multiple-network poroelastic theory: application to normal pressure hydrocephalus. Journal of Fluid Mechanics, 2011. 667: p. 188-215.

[4] Lambride, C., et al., Decompressive craniectomy of post-traumatic brain injury: an in silico modelling approach for intracranial hypertension management. Scientific Reports, 2020. 10(1): p. 18673.

[5] Mohamed Mokhtarudin, M.J. and S. Payne, Mathematical model of the effect of ischemia–reperfusion on brain capillary collapse and tissue swelling. Mathematical Biosciences, 2015. 263: p. 111-120.

[6] Mohamed Mokhtarudin, M.J., A. Shabudin, and S.J. Payne. Effects of Brain Tissue Mechanical and Fluid Transport Properties during Ischaemic Brain Oedema: A Poroelastic Finite Element Analysis. in 2018 IEEE-EMBS Conference on Biomedical Engineering and Sciences (IECBES). 2018.

[7] Cassot, F., et al., A novel three-dimensional computer-assisted method for a quantitative study of microvascular networks of the human cerebral cortex. Microcirculation, 2006. 13(1): p. 1-18.

[8] Penta, R. and D. Ambrosi, The role of the microvascular tortuosity in tumor transport phenomena. Journal of theoretical biology, 2015. 364: p. 80-97.

[9] Mascheroni, P. and R. Penta, The role of the microvascular network structure on diffusion and consumption of anticancer drugs. International Journal for Numerical Methods in Biomedical Engineering, 2017. 33(10): p. e2857.

[10] Shabudin, A., M.H. Jasni, and M.J.M. Mokhtarudin. Brain capillary geometry development for multiscale modelling study. in Engineering Technology International Conference (ETIC 2022). 2022.

[11] Mohamed Mokhtarudin, M.J., et al., Multiscale modelling of brain tissue oxygen and glucose dynamics in tortuous capillary during ischaemia-reperfusion. Applied Mathematical Modelling, 2022. 109: p. 358-373.

[12] Shabudin, A., et al. Multiscale Modelling of 3-Dimensional Brain Tissue with Capillary Distribution. in 2020 IEEE-EMBS Conference on Biomedical Engineering and Sciences (IECBES). 2021.

[13] Penta, R. and J. Merodio, Homogenized modeling for vascularized poroelastic materials. Meccanica, 2017. 52(14): p. 3321-3343.

[14] Davis, H. and D. Attwell, A tight squeeze: how do we make sense of small changes in microvascular diameter? The Journal of physiology, 2023.

15] Ray, L.A. and J.J. Heys, Fluid flow and mass transport in brain tissue. Fluids, 2019. 4(4): p. 196.

[16] Papadopol, C., Determination of soil hydraulic conductivity in nurseries and plantations. Tree planters' notes, 2005.

[17] Agarwal, N. and R.O. Carare, Cerebral Vessels: An Overview of Anatomy, Physiology, and Role in the Drainage of Fluids and Solutes. Frontiers in Neurology, 2021. 11.

[18] Biot, M.A., General theory of three-dimensional consolidation. Journal of applied physics, 1941. 12(2): p. 155-164.

[19] Majumder, S., M.T. Islam, and R. Righetti, Estimation of Mechanical and Transport Parameters in Cancers Using Short Time Poroelastography. IEEE Journal of Translational Engineering in Health and Medicine, 2022. 10: p. 1-11.

[20] Islam, M.T., et al., Non-invasive imaging of Young's modulus and Poisson's ratio in cancers in vivo. Scientific Reports, 2020. 10(1): p. 7266.